European Radiology (2019) 29:818–828
https://doi.org/10.1007/s00330-018-5614-9

MAGNETIC RESONANCE

Prospective comparison of diffusion-weighted MRI and dynamic Gd-EOB-DTPA-enhanced MRI for detection and staging of hepatic fibrosis in primary sclerosing cholangitis

S. Keller[1,2] · J. Sedlacik[3] · T. Schuler[1] · R. Buchert[1] · M. Avanesov[1] · R. Zenouzi[4] · A. W. Lohse[4] · H. Kooijman[5] · J. Fiehler[3] · C. Schramm[4] · J. Yamamura[1]

Received: 9 April 2018 / Revised: 26 May 2018 / Accepted: 15 June 2018 / Published online: 16 July 2018
© European Society of Radiology 2018

Abstract

Purpose To assess the diagnostic value of multiparametric magnetic resonance imaging (MRI) including dynamic Gd-EOB-DTPA-enhanced (DCE) and diffusion-weighted (DW) imaging for diagnosis and staging of hepatic fibrosis in primary sclerosing cholangitis (PSC) using transient elastography as a standard reference.

Material and methods Multiparametric MRI was prospectively performed on a 3.0-Tesla scanner in 47 patients (age 43.9±14.3 years). Transient elastography derived liver stiffness measurements (LSM), DCE-MRI derived parameters (hepatocellular uptake rate (Ki), arterial (Fa), portal venous (Fv) and total (Ft) blood flow, mean transit time (MTT), and extracellular volume (Ve)) and the apparent diffusion coefficient (ADC) were calculated. Correlation and univariate analysis of variance with post hoc pairwise comparison were applied to test for differences between LSM derived fibrosis stages (F0/F1, F2/3, F4). ROC curve analysis was used as a performance measure.

Results Both ADC and Ki correlated significantly with LSM (r= -0.614; $p<0.001$ and r= -0.368; $p=0.01$). The ADC significantly discriminated fibrosis stages F0/1 from F2/3 and F4 ($p<0.001$). Discrimination of F0/1 from F2/3 and F4 reached a sensitivity/specificity of 0.917/0.821 and 0.8/0.929, respectively. Despite significant inter-subject effect for classification of fibrosis stages, post hoc pairwise comparison was not significant for Ki ($p>0.096$ for F0/1 from F2/3 and F4). LSM, ADC and Ki were significantly associated with serum-based liver functional tests, disease duration and spleen volume.

Conclusion DW-MRI provides a higher diagnostic performance for detection of hepatic fibrosis and cirrhosis in PSC patients in comparison to Gd-EOB-DTPA-enhanced DCE-MRI.

Key Points

- *Both ADC and hepatocellular uptake rate (Ki) correlate significantly with liver stiffness (r= -0.614; p<0.001 and r= -0.368; p=0.01).*
- *The DCE-imaging derived quantitative parameter hepatocellular uptake rate (Ki) fails to discriminate pairwise intergroup differences of hepatic fibrosis (p>0.09).*
- *DWI is preferable to DCE-imaging for discrimination of fibrosis stages F0/1 to F2/3 (p<0.001) and F4 (p<0.001).*

Keywords Magnetic resonance imaging · Primary sclerosing cholangitis · Liver fibrosis · Diffusion magnetic resonance imaging · Gadolinium ethoxybenzyl DTPA

Electronic supplementary material The online version of this article (https://doi.org/10.1007/s00330-018-5614-9) contains supplementary material, which is available to authorized users.

✉ S. Keller
s.keller@uke.de; sarah.keller@charite.de

[1] Department of Diagnostic and Interventional Radiology and Nuclear Medicine, University Medical Center Hamburg-Eppendorf (UKE), Martinistr. 52, 20246 Hamburg, Germany

[2] Department of Radiology, Charité, Charitéplatz 1, 10117 Berlin, Germany

[3] Department of Neuroradiology, University Medical Center Hamburg-Eppendorf (UKE), Hamburg, Germany

[4] 1st Department of Medicine, University Medical Center Hamburg-Eppendorf (UKE), Hamburg, Germany

[5] Philips Medical Systems, MR Clinical Science, Hamburg, Germany

Abbreviations

ADC	Apparent diffusion coefficient
ALT	Alanine amino transferase
AP	Alkaline phosphatase
AST	Aspartate amino transferase
DCE	Dynamic contrast-enhanced
DWI	Diffusion-weighted imaging
EASL	European Association for the Study of the Liver
Fa	Arterial flow
Fi	Hepatic uptake fraction
FOV	Field-of-view
Fv	Portal venous flow
Gd-EOB-DTPA	Gadolinium ethoxybenzyl diethylenetriamine pentaacetic acid
GFR	Glomerular filtration rate
GGT	Gamma-glutamyl-transferase
IgG	Immunoglobulin G
Ki	Hepatocellular uptake rate
LSM	Liver stiffness measurements
METAVIR	Meta-analysis of histological data in viral hepatitis
MRI	Magnetic resonance imaging
MTT	Mean transit time
NEX	Number of excitations
PSC	Primary sclerosing cholangitis
ROC	Receiver operating characteristic
ROI	Region of interest
SD	Standard deviation
SPIR	Spectral inversion recovery
TE	Echo time
TR	Repetition time
TSE	Turbo spin echo
Ve	Extracellular volume

Introduction

Primary sclerosing cholangitis (PSC) is a chronic inflammatory liver disease characterised by progressive periductal fibrosis of the intra- and extrahepatic bile ducts, ultimately leading to biliary fibrosis, cirrhosis and hepatic failure [1, 2]. Recently, imaging modalities such as ultrasound transient elastography, diffusion-weighted MRI (DW-MRI) and dynamic contrast-enhanced MRI (DCE-MRI) have been applied for detection of hepatic fibrosis. Large cohort studies confirmed a high diagnostic performance of transient elastography for detection of liver fibrosis and cirrhosis in chronic liver disease [3–5], and transient elastography-derived liver stiffness measurements (LSM) have been categorised and validated according to the METAVIR [6]-derived scoring system [4]. In PSC patients, LSM-derived cut-off values for staging of fibrosis have been recently assessed by Corpechot et al [7], and these results were later validated in a larger cohort [8].

MR-DWI has been verified as another option for detection of fibrosis, especially in its moderate to advanced stages [9–11]. However, the apparent diffusion coefficient (ADC) may be affected by perfusion effects, liver inflammation, steatosis and iron overload [12].

A functional approach to liver fibrosis provides DCE-MRI, which has shown promising results to quantify hepatic fibrosis and cirrhosis either using extracellular [13–15] or hepatocyte-specific [16–18] contrast agents in patients and murine models. Above that, the dual-input two-compartment pharmacokinetic model presented by Sourbron et al [19] not only allows the quantification of parameters presenting hepatic blood flow, but also the hepatocellular uptake rate (Ki). Ki has been recently proposed as a potential biomarker of hepatic fibrosis, because this parameter not only correlates to fibrosis stage, but also distinguishes severe from non-severe fibrosis in subjects with chronic hepatitis [17].

So far, the diagnostic accuracy DW-MRI and DCE-MRI has not been compared in PSC patients. The aim of this prospective cross-sectional single-centre study was to assess the diagnostic performance of DW-MRI and DCE-MRI in PSC livers using multiparametric MRI and transient elastography derived LSM as standard reference.

Methods

Patients

Data of 47 consecutive patients (male:female 31:16 mean age 43.9±14.3 years) with diagnosed PSC according to EASL guidelines were prospectively collected between August 2014 and December 2015. In this Institutional Review Board-approved study, informed consent was obtained from all patients prior to the MRI examination. Patients with previous liver surgery, limited renal function (GFR < 30 ml/min/1.73 m^2) or other contraindications were excluded. Patients' demographic data are summarised in Table 1. Serum-based liver function tests (LFTs) (alkaline phosphatase (AP), alanine amino transferase (ALT), aspartate amino transferase (AST), gamma-glutamyl-transferase (GGT)), immunoglobulin G (IgG), platelets, bilirubin and albumin from each patient's last visit closest to the MRI examination [mean (standard deviation); 52.6 (65.5) days] were documented from medical records.

MR imaging

Multiparametric MRI was performed on a 3.0-Tesla scanner (Ingenia, Philips Medical Systems, Best, The Netherlands) equipped with a 24-channel body coil. First axial T2-

Table 1 Patients demographics separated by transient elastography derived stages of hepatic fibrosis

		Fibrosis stage		
	Overall (N=47)	F1/0 (N=28)	F2/3 (N=14)	F4 (N=5)
Gender	N (%)			
Female	16 (34)	9 (32.1)	6 (42.9)	2 (40)
Male	31 (66)	19 (67.9)	8 (57.1)	3 (60)
	Mean ± standard deviation			
Age (years)	43.9 ± 14.3	41.5 ± 13.8	50.8 ± 15.4	40.0 ± 10.1

weighted imaging for anatomical orientation was performed over the epigastric region. For DCE-imaging a Dixon fat-suppressed T1-weighted three-dimensional (3D) FFE (TR/TE1/TE2/FA 3.9 ms/1.15 ms/2.3 ms/20°, field of view (FOV) 400 x 300 x 175 mm (RL/AP/FH), 70 slices, slice thickness 3 mm with slice oversampling factor of 1.6 and SENSE factor 5) with 140 scans covering the whole liver, was performed. Six volumes were imaged pre-contrast for baseline calculations, followed by 134 volumes with a step-wise increase in sampling intervals 3 s after intravenous administration of 0.1 ml/kg Gd-EOB-DTPA 0.25 mmol/ml (Primovist; Bayer) at an infusion rate of 2 ml/s followed immediately by a bolus of 20 ml saline (NaCl 0.9%) using a power injector (Spectris MR injector System, Medrad). The volumes were imaged with a navigated respiratory compensation over a time period of 12 min (actual scan time 7 min). To ensure steady-state T1 weighting in the centre of the k-space, the k-space order was outside-to-centre, and the sequence was preceded by a non-volume-selective saturation pulse, which helps to reach steady state over a large range of T1 values (50–2,000 ms) within the first 200 ms of the sequence, avoiding inflow-effects and also avoiding signal variations due to irregular respiratory intervals.

DW-MRI

Based on the T2-weighted images a transverse, respiratory-gated single-shot spin-echo echo planar imaging sequence (SS-SE EPI) was generated covering the whole liver (TR 1,985 ms; TE 69 ms; FOV 400 x 400 mm; voxel size 1.79 x 1.79 x 3.0 mm; slice thickness 5.0 mm; intersection gap 0 mm; consecutive b-factors of 0, 50, 100, 200, 400, 800 s/mm^2; average 35 slices; and number of excitations (NEX) 2). The scan duration was approximately 5 min. Fat suppression was performed using spectral inversion recovery (SPIR). For ADC-map calculation, a starting b-value of 50 s/mm^2 was used to suppress the contribution of the vascular signal. The diffusion weighting was performed with a trace weighted sequence type (three orthogonal directions).

Transient elastography

Hepatic fibrosis was diagnosed using transient elastography (Fibroscan, EchoSens) as reported previously [20]. Fibroscan was performed within an interval of ±7 months (mean (standard deviation) 91.4 (72.4) days) to MRI. The target area of the right liver lobe was determined by ultrasonography to be 6 cm deep without major vascular structures. LSM cut-off values for discrimination of fibrosis stages were used according to Corpechot et al [7] with absent or mild fibrosis (F0/1; stiffness ≤ 8.5 kPa); significant to severe fibrosis (F2/3; stiffness ≥8.6 kPa to ≤ 14.3 kPa); and cirrhosis (F4; stiffness ≥14.4 kPa).

DCE-MRI post-processing

Image analysis was performed by two radiologists with 4 years and 5 years of experience in abdominal MRI blinded to patients' data. Arterial and venous inputs were defined by regions of interest (ROIs) placed over the suprarenal aorta and the intra- and extrahepatic portal vein, respectively (Fig. 1a,b). To avoid residual inflow effects in the aorta, the arterial input was measured in the lower third of the transversal 3D volume, where the blood has travelled at least 10 cm through the imaging volume, corresponding to 100 ms presuming a maximum blood flow of 100 cm/s, which corresponds to the time in which steady state is reached (see Methods section). Three ROIs were then located in liver segments according to areas analysed by transient elastography (liver segments V/VI) (Fig. 1c). Signal intensity changes from each ROI were fitted to a dual-input, two-compartment uptake model [19] using an in-house software written in MATLABVR (Mathworks). Primarily derived DCE-MRI parameters Ki (/100 min), extracellular volume (Ve; ml/100 ml), portal venous flow (Fv; ml/min/100 ml), and arterial flow (Fa; ml/min/100 ml) were used to calculate the parameters: total blood flow (Ft (ml/min/100 ml) = Fa + Fv), extracellular mean transit time (MTT (sec) = Ve / (Fa + Fv + Ki)), and hepatic uptake fraction (Fi (%) = Ki / (Fa + Fv + Ki)).

DW-MRI post-processing

ADC maps were generated using custom MR software (Philips Medical Systems) on the base of a voxel-wise calculation interpolated to a 256 x 256 mm^2 matrix. The two raters reviewed the images and measured liver ADC values by drawing three ROIs (mean size 173 mm^2, range 121–237 mm^2) in areas corresponding to transient elastography and DCE-MRI as exemplified in Fig. 2. Vessels and lesions were excluded.

MR imaging parameters

Conventional MR imaging parameters, which are frequently associated with portal hypertension, such as collateral

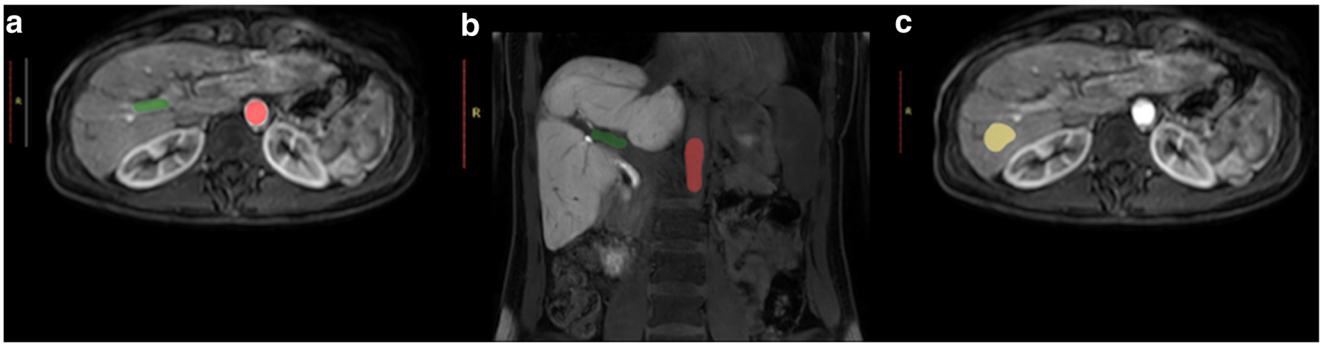

Fig. 1 Examples of region of interest (ROI) placement for arterial (red) and portal venous (green) output function and DCE quantitative parameters of function on the liver parenchyma (yellow) on axial (**a**, **c**) dynamic contrast-enhanced fat-saturated T1-weighted images with orientation on coronal (**b**) contrast enhanced image (late phase, 20 min after intravenous contrast agent injection)

circulation, ascites and oesophageal varices were graded using a nominal scale by two radiologists in consensus. The spleen volume was calculated with OsiriX software (OsiriX Lite v.9.0) on T2-weighted axial image sets with a slice thickness of 3 mm.

Statistics

Continuous data are presented as mean and standard deviation. D'Agostino-Pearson omnibus test was applied to test for normal distribution. Pearson's correlation and Bland-Altman analysis were used to assess inter-rater reliability with respect to quantitative ADC and DCE parameters. The criteria of Portney and Watkins [21] were used to judge the strength of the correlation coefficients as follows: little to no relationship ($r \leq 0.25$), fair degree of relationship ($r = 0.26–0.50$), moderate-to-good relationship ($r = 0.51–0.75$) and good-to-excellent relationship ($r \geq 0.76$). ADC and DCE parameters were analysed for correlation with LSM, spleen size, LFTs and MR imaging findings using Pearson's correlation or logistic regression models in case of nominal scaling. Partial correlation analysis corrected for potential effects of age and gender. Univariate analysis of variance was used to test ADC and DCE parameters for differences between the fibrosis stages (F0/1, F2/3, F4). In case of a significant inter-subject effect on the classification of a fibrosis stage, the Scheffé or the Tamhane post hoc test (according to the result of the Levene test of homogeneity of variances) was applied for pairwise comparison of fibrosis stages. These tests are deliberately conservative to reduce the probability of too many significant differences arising by chance. Receiver operating characteristic (ROC) curve analysis evaluated the diagnostic accuracy of ADC and Ki for discrimination of F0/1 from F2/3 and F4 and the Youden-Index determined the optimal cut-off values. All statistical analyses were performed with IBM SPSS 24 (Armonk, NY, USA).

Results

Inter-rater reliability

Inter-rater reliability with respect to all quantitative DW-MRI- and DCE-MRI-derived parameters Ki and Ve was excellent.

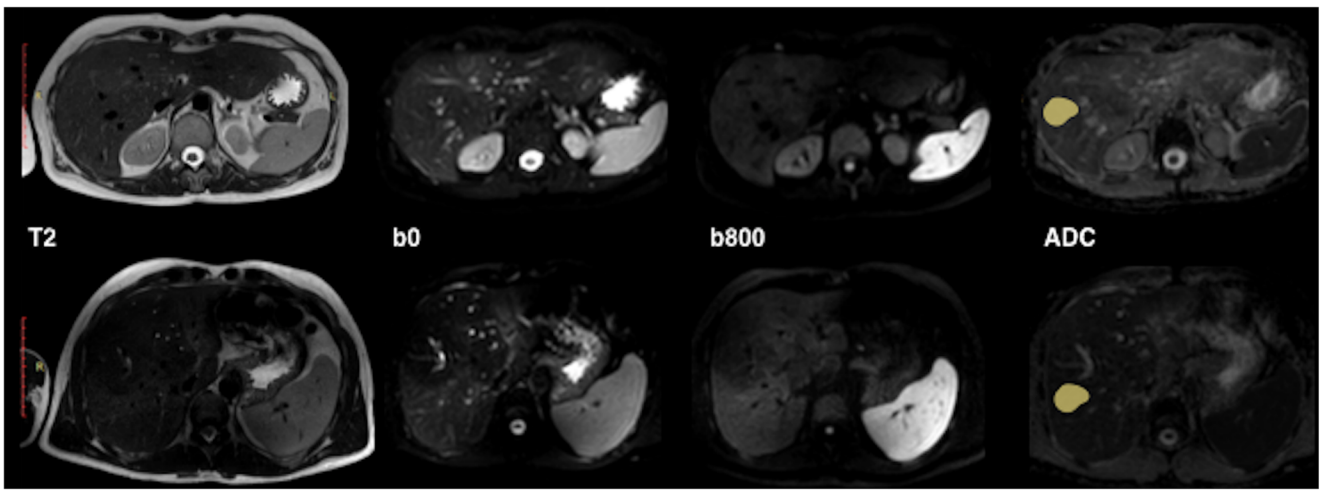

Fig. 2 Axial DWI images and ADC-map of two PSC patients. Left to right: T2-weighted image, DWI b=0; b=800; and ADC-map including example of region-of-interest. Upper row: 34-year-old female patient fibrosis stage F0/1; lower row: 35-year-old male patients fibrosis stage F4

The inter-rater reliability of Fv and Fa was good to moderate. For all data, no systematic offset (according to paired t-test) was detected. Details are summarised in Table 2 and Fig. 3.

Transient elastography-derived LSM and stages of fibrosis

Patients were subcategorised according to transient elastography-derived stages of fibrosis proposed by Corpechot et al [7]: F0/1: (N= 28); F2/3: (N= 14); and F4: (N= 5). LSM correlated with disease duration, AST, GGT, AP, IgG, platelets, albumin and spleen volume (see Online Supplementary Material, Table 1). No association of LSM and imaging parameters of portal hypertension (ascites, oesophageal varices, collateral circulation) was observed.

Correlation of ADC with LSM

ADC values according to fibrosis stage are included in Table 3. The ADC correlated significantly with LSM (r= -0.614; $p<0.001$). Post hoc comparison testing showed significant differences in discrimination of: F0/1 from F2/3 ($p<0.001$) and F4 ($p<0.001$). No statistical significance was achieved for discrimination of F2/3 to F4 ($p=0.95$) (Table 4).

Correlation of DCE-MRI with LSM

Figure 4 gives an example of different signal intensities obtained on DCE maximum intensity projection images (MIP) in patients staged F0/1 and F3. As exemplified in Fig. 4, the overall signal intensity of F0/1 liver parenchyma was higher compared to F3. However, we did not observe significant associations of LSM with Fa, Fv, Ft and MTT ($p\geq0.24$). Out of all parameters analysed, Ki (r= -0.368; $p=0.01$) and Fi (r= -0.342; $p=0.02$) significantly correlated with LSM and with ADC (r= 0.4; $p=0.006$; r= 0.38; $p=0.012$, respectively) (Table 3). This effect was stable considering potential effects of age and gender. Despite significant inter-subject effects, Ki did not achieve significant discrimination of fibrosis stages on pairwise post hoc comparison testing ($p\geq0.096$) (Table 4). Fi consistently correlated with LSM but did not achieve significant inter-subject effect on classification of fibrosis stages. The boxplot in Fig. 5 gives an illustration of ADC, Ki and Fi categorised by stages of fibrosis. Ve remained stable at different fibrosis stages.

Table 2 Inter-rater reliability of diffusion-weighted imaging (DWI) and dynamic contrast-enhanced imaging (DCE) derived quantitative parameters (ADC, Ki, Ve, Fv, and Fa)

	ADC	Ki	Ve	Fv	Fa
Correlation coefficient (r)	0.804	0.946	0.869	0.602	0.517
p-value	0.302	0.608	0.907	0.612	0.780

$p< 0.05$ statistically significant

ADC apparent diffusion coefficient ($mm^2/s\ x10^{-3}$), *Ki* hepatocellular uptake fraction (/100/min), *Ve* extracellular volume (ml/100 ml), *Fv* portal venous flow (ml/min/100 ml), *Fa* arterial flow (ml/min/100 ml)

Receiver operating characteristic curves of ADC

ROC curve analysis of ADC as a performance measure in discriminating F2/3 and F4 from F0/1 was performed (Fig. 6). The AUC for discrimination of F1/0 from F2/3 was 0.926 (95% confidence interval (CI) (0.847–1.0); $p<0.001$). For discrimination of F0/1 from F2/3 the ADC cut-off of 1.14 $mm^2/s\ x10^{-3}$ achieved a sensitivity of 0.917 and a specificity of 0.821. For discrimination of F0/1 from F4 the AUC of ADC was 0.914 (95% CI (0.799–1.0); $p=0.004$). The cut-off value of 1.09 $mm^2/s\ x10^{-3}$ reached a sensitivity of 0.8 and a specificity of 0.929. A higher sensitivity of 1.0 was achieved at cost of a lower specificity of 0.714 using a cut-off value of 1.17 $mm^2/s\ x10^{-3}$.

Receiver operating characteristics curves of Ki

Based on significant inter-subject effect testing for classification of fibrosis stages ($p<0.001$), ROC analysis was performed (Fig. 6). The AUC of Ki for discrimination of F0/1 from F2/3 was 0.632 (95% CI (0.442–0.823); $p=0.179$). The cut-off value of Ki= 3.55/100/min reached a sensitivity of 0.692 and a specificity of 0.481. The AUC for discrimination of F0/1 from F4 was 0.756 (95% CI (0.498–1.0); $p=0.073$). The cut-off value of Ki= 2.55/100/min reached a sensitivity of 0.6 and a specificity of 0.926. A higher sensitivity of 0.8 was achieved using a cut-off value of Ki= 3.41/100/min, however by compromising the specificity to 0.519.

Correlation of Ki and ADC with LFTs and MR imaging parameters

Pearson correlation of LFTs with Ki and ADC are illustrated in Table 5. ADC inversely correlated with AP (r= -0.32; $p=0.031$), GGT (r= -0.34; $p=0.021$) and IgG (r= -0.37; $p=0.011$). Ki inversely correlated with AST (r= -0.30; $p=0.044$), AP (r= -0.30; $p=0.049$), GGT (r= -0.33; $p=0.027$), and bilirubin (r= -0.38; $p=0.01$). Significant inverse correlation was observed of spleen volumes with ADC (r= -0.34; $p=0.02$) and Ki (r= -0.36; $p= 0.012$). MR imaging parameters were rated as follows: collateral circulation N=11, oesophageal varices N= 2, ascites N=0 patients. Logistic regression models showed no significant association with Ki and ADC (Table 5).

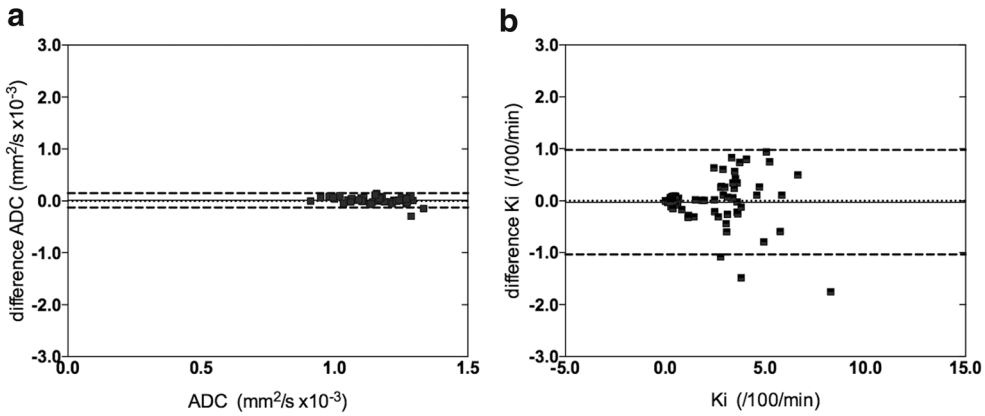

Fig. 3 Inter-rater variability of the apparent diffusion coefficient (ADC) and hepatocellular uptake rate (Ki). Small dotted lines represents the bias, dashed lines the 95% limits of agreement. (**a**) ADC (bias 0.01; 95% limits of agreement -0.13 to 0.15); (**b**) Ki (bias -0.03; 95% limits of agreement -1.04 to 0.98)

Discussion

This multiparametric study compares the diagnostic performance of Gd-EOB-DTPA-enhanced DCE-MRI and DWI-MRI for detection and discrimination of hepatic fibrosis in PSC patients using transient elastography as a standard reference.

Applying an already validated dual-input two-compartment model, the quantitative parameter Ki correlated inversely with LSM, but did not perform well in discriminating fibrosis stages F0/1 to F2/3 or F4. The cut-off value of Ki= 2.55/100/min discriminated F0/1 from F4 with a sensitivity of 0.6 and a specificity of 0.926. A higher sensitivity of 0.8 was achieved by lowering the specificity to 0.519 using a cut-off value of Ki= 3.41/100/min. Fi correlated with LSM, but reached no significant inter-subject difference for classification of fibrosis stages. A study reporting an inverse correlation of hepatic Ki with histopathological stages of fibrosis (r= -0.55; 95% CI (0.79,-0.14); p=0.01) has been published previously by Juluru et al [22] in patients with chronic hepatitis and controls. In contrast to our study, Fi did not correlate to liver fibrosis, which may be explained as a result of the small sample size (N= 22) or differences in blood flow parameters (Fv and Fa) influenced by technical settings such as injection flow of Gd-EOB-DTPA (1.5 ml/s vs. 2 ml/s in our study) as well as cardiopulmonary conditions of the study group. As demonstrated in a previous study by Ning et al [23] of patients admitted to MRI for variable liver lesions, using a dual-input two-compartment model, Ki inversely correlated to bilirubin levels (r = -0.52, p= 0.015). The finding that Ki is negatively associated with bilirubin is in compliance with results of our study. In contrast to the study cohort of Juluru et al, cholestasis is a common finding in PSC. Following injection and uptake via organic anion-transporting polypeptides (OATP),

Table 3 ADC and quantitative DCE-MRI parameters subcategorised according to transient elastography derived stages of fibrosis F0/1, F2/3 and F4

Parameter				Fibrosis Stage		
	Overall (N=47)	Correlation with LSM r [95% confidence interval]	p-value	F1/0 (N=28)	F2/3 (N=14)	F4 (N=5)
ADC (mm^2/s x10^{-3})	**1.149 ± 0.1**	**-0.614 [-0.76 to -0.39]**	**<0.001**	**1.207 ± 0.07**	**1.057 ± 0.06**	**1.044 ± 0.1**
DCE-Parameters						
Fa (ml/min/100ml)	41.35 ± 18.2	-0.119 [-0.40 to 0.18]	0.43	40.35 ± 21.0	46.49 ± 11.4	33.43 ± 7.3
Fv (ml/min/100ml)	72.53 ± 29.0	0.180 [-0.12 to 0.45]	0.24	73.90 ± 26.6	58.57 ± 21.9	101.42 ± 31.4
Ft (ml/min/100ml)	113.9 ± 29.0	0.104 [-0.20 to 0.39]	0.49	112.8 ± 28.1	105.1 ± 21.5	134.85 ± 33.8
Ve (ml/100ml)	8.72 ± 1.8	0.09 [-0.21 to 0.37]	0.55	8.86 ± 1.67	8.76 ± 2.22	9.50 ± 1.9
Ki (/100/min)	**3.52 ± 1.98**	**-0.368 [-0.60 to -0.08]**	**0.01**	**4.10 ± 2.07**	**2.69 ± 1.65**	**2.51 ± 1.10**
Art (%)	37.01 ± 15.6	-0.112 [-0.40 to 0.18]	0.44	35.38 ± 16.3	45.37 ± 11.7	25.86 ± 7.5
Port (%)	62.99 ± 15.6	0.13 [-0.18 to 0.40]	0.44	64.62 ± 16.3	54.63 ± 11.7	74.14 ± 7.6
Fi (%)	**3.18 ± 1.8**	**-0.342 [-0.58 to -0.05]**	**0.02**	**3.69 ± 2.1**	**2.70 ± 1.6**	**2.0 ± 1.01**
MTT (sec)	7.9 ± 3.0	-0.06 [-0.35 to 0.23]	0.7	8.35 ± 3.6	8.48 ± 2.8	7.29 ± 1.0

Bold type indicates significant correlation ($p \leq 0.05$); parameters are shown as mean ± standard deviation

Abbreviations: ADC, apparent diffusion coefficient; DCE, dynamic contrast-enhanced; Fa, absolute arterial blood flow; Fv, absolute portal venous blood flow; Ft, total blood flow; Ve, extracellular volume; Ki, hepatocellular uptake rate; Art, arterial flow fraction; Port, portal venous flow fraction; Fi, hepatocellular uptake fraction; MTT, extracellular mean transit time.

Table 4 Post-hoc testing for discrimination of fibrosis stages (F0-4) using the apparent diffusion coefficient ADC (mm^2/s x10^{-3}) and hepatocellular uptake rate Ki (/100/min)

Fibrosis stage (A)	Fibrosis stage (B)	Difference mean (A-B)	Standard error	*p*-value	95% confidence interval
ADC					
F0/1	**F2/3**	**0.149**	**0.025**	**< 0.001**	**0.085 to 0.214**
	F4	**0.162**	**0.036**	**< 0.001**	**0.071 to 0.253**
F2/3	F4	0.013	0.039	0.95	-0.214 to -0.085
Ki					
F0/1	F2/3	1.414	0.634	0.096	-0.196 to 0.302
	F4	1.592	0.915	0.232	-0.729 to 0.391
F2/3	F4	0.179	0.99	0.984	-0.233 to 0.269

Bold type indicates significant mean difference ($p \leq 0.05$)

intracellular transport of Gd-EOB-DTPA is mediated by the glutathione-S-transferase transport system and both bilirubin and Gd-EOB-DTPA share a high affinity for its receptor [24]. Above that, in advanced liver cirrhosis the number of functioning hepatocytes is reduced together with its connected bilirubin and Gd-EOB-DTPA pathways [25]. In line with Juluru et al [22], the Ve remained unchanged at different stages of fibrosis. A possible explanation could be the longer intracellular residence time of Gd-EOB-DTPA exceeding the applied DCE-MR imaging acquisition time, so that the loss of tracer out of the intracellular space could be assumed to be negligible [19]. A general shortcoming of the model used by Sourbron [19] and the present study is the presumed linearity between the contrast agent concentration and the relative signal enhancement. This linearity is violated towards higher concentrations (leading to very short T1-values), in particular with Gd-EOB-DTPA, which has a higher T1-relaxivity in plasma (6.2 L $mmol^{-1}s^{-1}$) compared to Gd-DTPA (3.7 L $mmol^{-1}s^{-1}$). In addition, unavoidable RF-field inhomogeneities at 3.0 Tesla may lead to locally smaller RF-pulse angles, increasing this non-linearity [26]. This shortcoming could also have led to less significance of our DCE results.

The diagnostic efficacy of DW-MRI for staging of hepatic fibrosis has been compared in various studies to METAVIR histopathological stages of fibrosis [27, 28], transient elastography [29] and MR-elastography (MRE) [30, 31]. Possibly due to the increase of intrahepatic connective tissue supposedly lowering the hepatic blood flow [32] and diffusion capacities [33], diffusion becomes restricted in the presence of fibrosis, which goes along with a negative correlation of the hepatic ADC with LSM. This association is consistent and efficient in differentiating multiple stages of fibrosis (F0/1 from F2/3 and F4). (Table 5 and Online Supplementary Material, Table 1). Correlation between ADC, Ki, LSM revealed a consistent significant association with alkaline phosphatase (AP), which is of great interest as this parameter was already identified as promising surrogate to predict risk of cholangiocarcinoma and overall disease outcome in patients with PSC [34–36]. In addition, LSM, ADC and Ki were significantly associated with spleen volumes, which underlines results of previous studies where spleen volumes were correlated with liver stiffness and outcome of PSC [8, 37]. LSM, ADC and Ki were not associated with imaging parameters frequently observed with portal hypertension, which may be

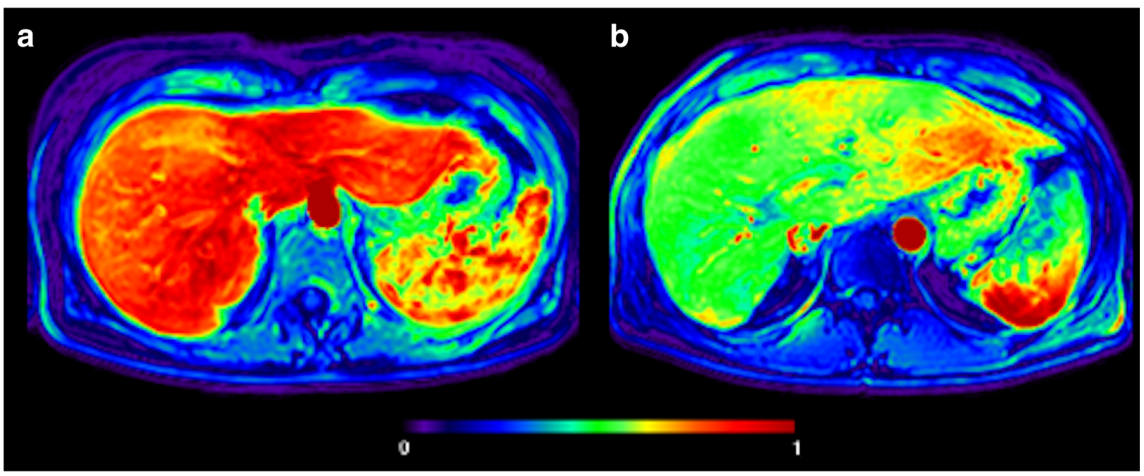

Fig. 4 Axial dynamic maximum intensity projection (MIP) of Gd-EOB-DTPA-enhanced scans. (**a**) Fibrosis stage F 0/1. (**b**) Fibrosis stage F3

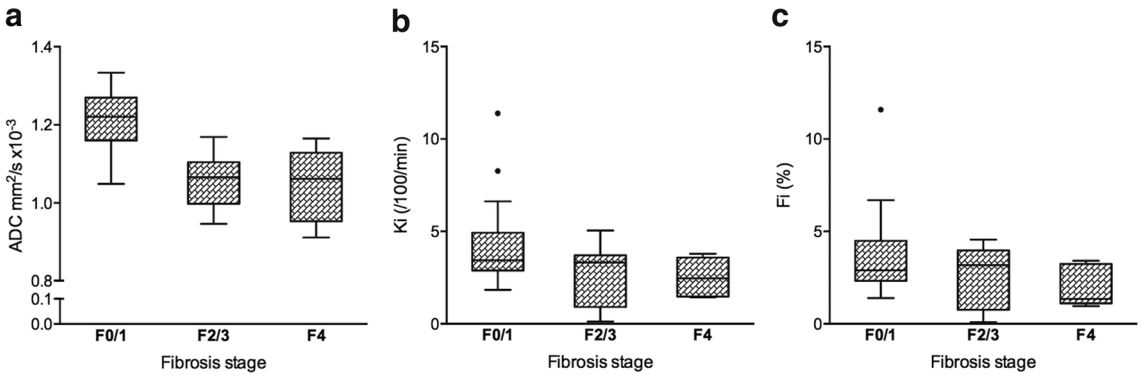

Fig. 5 Boxplot of liver apparent diffusion coefficient (ADC) (**a**), hepatocellular uptake rate (Ki) (**b**) and hepatocellular uptake fraction (Fi) (**c**) categorised by fibrosis stage. Centreline shows the medians, boxplot limits the 25th to 75th percentiles. Whiskers extend 1.5 times the interquartile range from 25th to 75th percentile; outliers are represented by dots

related to the small number of cirrhotic patients included into this study.

The diagnostic superiority of transient elastography over DW-MRI has been confirmed in previous studies [29] and is well reflected in the strong association of LSM with LFTs in this study. The proven validity of transient elastography is one reason behind the rationale to use this modality as a standard reference in our study, especially as biopsies obtained in an appropriate time interval to imaging are scarce and histopathology is not regarded as a standard procedure for diagnosis of non-small-duct PSC in current guidelines [38]. However, recent studies comparing transient elastography and MRE demonstrated a higher diagnostic performance of MRE for discriminating fibrosis in patient cohorts of variable chronic hepatic disease [15, 39]. If these results are validated in PSC cases, MRE could replace the here employed MRI modalities of fibrosis staging.

Other MR modalities proposed for diagnosis of fibrosis, which have not been evaluated in our study, are intravoxel incoherent motion (IVIM) DW-MRI and T1 mapping. IVIM is an upcoming extension of DW-MRI, taking into account both the molecular diffusion and incoherent motion of water molecules in the capillary network known as pseudo-diffusion. Because accumulation of the extracellular matrix in fibrosis affects both true diffusion and microcirculation, IVIM parameters pseudo-diffusion coefficient (D*), diffusion coefficient (D), perfusion fraction (P) and ADC show associations with fibrosis but seem not to have the diagnostic accuracy to detect and stage fibrosis as a single imaging modality [14, 40, 41]. T1 mapping directly measures the T1 relaxation time by milliseconds, which depends on the molecular environment of water molecules in tissue. Recent studies evaluated T1 mapping in liver fibrosis, demonstrating that T1 relaxation times constantly increase with severity of liver cirrhosis [42, 43]. These studies showed a diagnostic performance comparable

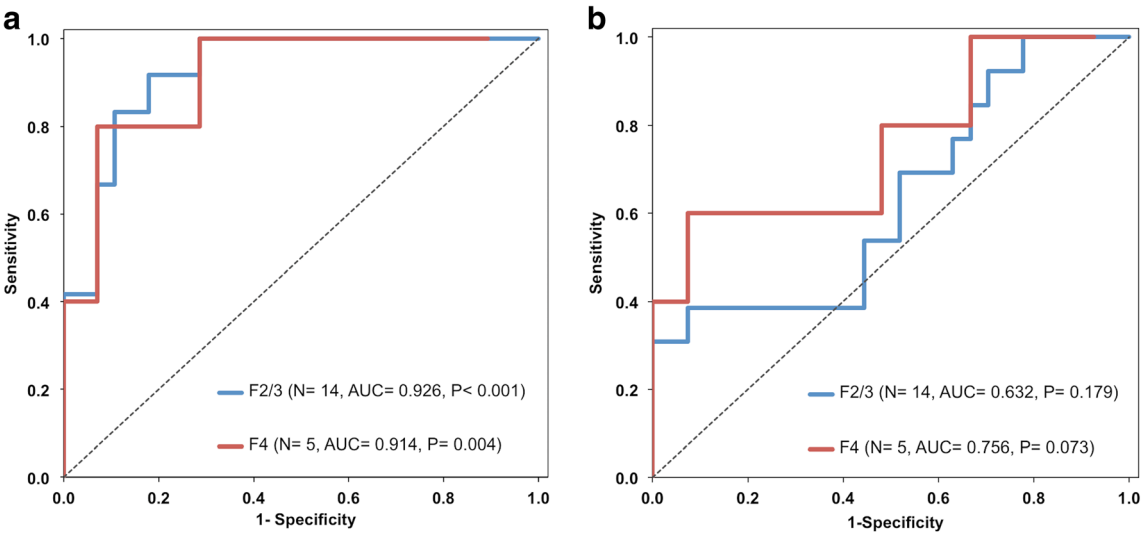

Fig. 6 Receiver operating characteristic (ROC) curves of the liver apparent diffusion coefficient (ADC) (**a**) and hepatocellular uptake rate (Ki) (**b**) for discriminating stages of fibrosis F0/1 to F2/3 and F4HER85614

Table 5 Correlation between Ki and ADC with LFTs, spleen size and MR-imaging parameters

LFT	Ki		ADC	
	r [95% confidence interval]*	*p*-value	r [95% confidence interval]*	*p*-value
AST (U/L)	**-0.30 (-0.55 to -0.01)**	**0.044**	-0.21 (-0.47 to 0.08)	0.150
ALT (U/L)	-0.22 (-0.49 to 0.08)	0.139	-0.17 (-0.44 to 0.12)	0.253
GGT (U/L)	**-0.33 (-0.57 to -0.04)**	**0.027**	**-0.34 (-0.57 to 0.06)**	**0.021**
AP (U/L)	**-0.30 (-0.54 to -0.001)**	**0.049**	**-0.32 (-0.55 to -0.03)**	**0.031**
IgG (g/L)	-0.15 (-0.43 to 0.16)	0.344	**-0.37 (-0.60 to -0.09)**	**0.011**
Bil (mg/dl)	**-0.38 (-0.61 to -0.10)**	**0.010**	-0.26 (-0.51 to 0.03)	0.073
Alb (g/L)	0.14 (-0.17 to 0.42)	0.374	0.29 (-0.003 to 0.53)	0.053
TC /nl	0.24 (-0.06 to 0.50)	0.115	0.16 (-0.14 to 0.43)	0.287
Imaging parameters	r (95% confidence interval)*	*p*-value	r (95% confidence interval)*	*p*-value
Spleen volume (cm^3)	**-0.36 (-0.59 to -0.07)**	**0.012**	**-0.34 (-0.57 to -0.06)**	**0.020**
	OR**	*p*-value	OR**	*p*-value
Collateral veins	0.001	0.964	0.001	0.966
Oesophageal varices	1.1	0.728	0.67	0.935

Bold type indicates significant values ($p \leq 0.05$)

*Based on Pearson correlation

**Based on binary logistic regression models

LFT liver function tests, *IgG* Immunoglobulin G, *AP* alkaline phosphatase, *AST* aspartate amino transferase, *ALT* alanine amino transferase, *GGT* gamma-glutamyltransferase, *Bil* bilirubin, *Alb* albumin, *TC* thrombocytes, *r* Pearson coefficient, *OR* odds ratio

to or above ADC for discrimination of fibrosis stages in patients with variable liver disease [44] and rodent models [45]. In PSC patients a significant correlation of T1 reduction to clinical scores of disease severity (MELD, Mayo risk score) and LFTs has been described recently [46]. However, the diagnostic performance of T1 mapping for detection and staging of fibrosis in PSC has not been evaluated so far. The delayed-phase relative liver enhancement (RLE) of extracellular gadolinium-based contrast agents (GBCA) has been recently been proposed as another correlate measure of liver fibrosis in PSC patients. Quantification of extracellular RLE is applicable in the clinical setting where standard contrast-enhanced follow-up scans are routinely performed for surveillance of malignancy and dominant biliary strictures in PSC patients. In comparison to hepatocyte-specific DCE-MRI, the latter technique has the advantages of time- and cost efficacy. In a previous study the delayed-phase RLE significantly discriminated histologically derived stages of fibrosis F2 (β= 35.13; p=0.007) and F3-4 (β= 69.24; p<0.001) from F0 based on linear regression models [47]. The association of delayed-phase extracellular GBCA enhancement patterns and histologically derived fibrosis was further evaluated by another study in chronic and active hepatitis [r= 0.96; 95% CI (0.941 to 0.976)] [48]. However, none of these studies has so far compared extracellular delayed-phase DCE-MRI to DW-MRI.

One of the limitations of this present study is the lack of correlation to histopathological data, although transient elastography is well investigated and correlates with pathological results in prior studies [4, 6, 49]. For further investigation the histological assessment of biopsy specimens can be performed MRI-guided to be more precise and thus could be an object of future studies. Although we do not expect major changes of fibrosis stages within the chosen maximal time interval of 7 months between transient elastography and MRI, we cannot completely exclude that a more precise correlation of data could have been obtained if modalities were performed within one consultation. Another point is the study design, which was performed at a single centre. Since this is the first study of its kind, a multicentre study for data validation would be preferable in the future.

In conclusion, the findings of this multiparametric study demonstrate that DW-MRI is superior to Gd-EOB-DTPA-enhanced DCE-MRI in diagnosing and differentiating several stages of hepatic fibrosis in PSC patients and could be a useful non-invasive and fast add-on to current follow-up MRI protocols. Nevertheless, there are several other evolving MR modalities for staging of fibrosis, such as T1 mapping, IVIM and MRE, which have so far not been evaluated in PSC cohorts and could possibly outperform DCE-MRI, DW-MRI and transient elastography. A multicentre multiparametric MRI study comparing DW-MRI, MRE, IVIM, T1 mapping and transient elastography in comparison to histopathological results would be the best way to generate a diagnostic standard of fibrosis staging in PSC patients.

Funding A.W. Lohse and C. Schramm were funded by the Deutsche Forschungsgemeinschaft (DFG) (SFB841 and KFO306).

Compliance with ethical standards

Guarantor The scientific guarantor of this publication is J. Yamamura.

Conflict of interest The authors of this manuscript declare relationships with the following companies: Philips Healthcare (H. Kooijman).

Statistics and biometry One of the authors has significant statistical expertise (R. Buchert).

Informed consent Written informed consent was obtained from all subjects in this study.

Ethical approval Institutional Review Board approval was obtained.

Methodology
- prospective
- experimental study
- performed at one institution

References

1. Portmann B, Zen Y (2012) Inflammatory disease of the bile ducts-cholangiopathies: liver biopsy challenge and clinicopathological correlation. Histopathology 60:236–248
2. Kovac JD, Weber MA (2016) Primary Biliary Cirrhosis and Primary Sclerosing Cholangitis: an Update on MR Imaging Findings with Recent Developments. J Gastrointestin Liver Dis 25:517–524
3. Ziol M, Handra-Luca A, Kettaneh A et al (2005) Noninvasive assessment of liver fibrosis by measurement of stiffness in patients with chronic hepatitis C. Hepatology 41:48–54
4. Castera L, Vergniol J, Foucher J et al (2005) Prospective comparison of transient elastography, Fibrotest, APRI, and liver biopsy for the assessment of fibrosis in chronic hepatitis C. Gastroenterology 128:343–350
5. Foucher J, Chanteloup E, Vergniol J et al (2006) Diagnosis of cirrhosis by transient elastography (FibroScan): a prospective study. Gut 55:403–408
6. Bedossa P, Poynard T (1996) An algorithm for the grading of activity in chronic hepatitis C. The METAVIR Cooperative Study Group. Hepatology 24:289–293
7. Corpechot C, Gaouar F, El Naggar A et al (2014) Baseline values and changes in liver stiffness measured by transient elastography are associated with severity of fibrosis and outcomes of patients with primary sclerosing cholangitis. Gastroenterology 146:970–979 quiz e915-976
8. Ehlken H, Wroblewski R, Corpechot C et al (2016) Validation of Transient Elastography and Comparison with Spleen Length Measurement for Staging of Fibrosis and Clinical Prognosis in Primary Sclerosing Cholangitis. PLoS One 11:e0164224
9. Taouli B, Tolia AJ, Losada M et al (2007) Diffusion-weighted MRI for quantification of liver fibrosis: preliminary experience. AJR Am J Roentgenol 189:799–806
10. Taouli B, Chouli M, Martin AJ, Qayyum A, Coakley FV, Vilgrain V (2008) Chronic hepatitis: role of diffusion-weighted imaging and diffusion tensor imaging for the diagnosis of liver fibrosis and inflammation. J Magn Reson Imaging 28:89–95
11. Lewin M, Poujol-Robert A, Boelle PY et al (2007) Diffusion-weighted magnetic resonance imaging for the assessment of fibrosis in chronic hepatitis C. Hepatology 46:658–665
12. Faria SC, Ganesan K, Mwangi I et al (2009) MR imaging of liver fibrosis: current state of the art. Radiographics 29:1615–1635
13. Li Z, Sun J, Chen L et al (2016) Assessment of liver fibrosis using pharmacokinetic parameters of dynamic contrast-enhanced magnetic resonance imaging. J Magn Reson Imaging 44:98–104
14. Patel J, Sigmund EE, Rusinek H, Oei M, Babb JS, Taouli B (2010) Diagnosis of cirrhosis with intravoxel incoherent motion diffusion MRI and dynamic contrast-enhanced MRI alone and in combination: preliminary experience. J Magn Reson Imaging 31:589–600
15. Dyvorne HA, Jajamovich GH, Bane O et al (2016) Prospective comparison of magnetic resonance imaging to transient elastography and serum markers for liver fibrosis detection. Liver Int 36:659–666
16. Nilsson H, Blomqvist L, Douglas L et al (2013) Gd-EOB-DTPA-enhanced MRI for the assessment of liver function and volume in liver cirrhosis. Br J Radiol 86:20120653
17. Juluru K, Talal AH, Yantiss RK et al (2016) Diagnostic accuracy of intracellular uptake rates calculated using dynamic Gd-EOB-DTPA-enhanced MRI for hepatic fibrosis stage. J Magn Reson Imaging. https://doi.org/10.1002/jmri.25431
18. Zhang W, Kong X, Wang ZJ, Luo S, Huang W, Zhang LJ (2015) Dynamic Contrast-Enhanced Magnetic Resonance Imaging with Gd-EOB-DTPA for the Evaluation of Liver Fibrosis Induced by Carbon Tetrachloride in Rats. PLoS One 10:e0129621
19. Sourbron S, Sommer WH, Reiser MF, Zech CJ (2012) Combined quantification of liver perfusion and function with dynamic gadoxetic acid-enhanced MR imaging. Radiology 263:874–883
20. Sandrin L, Fourquet B, Hasquenoph JM et al (2003) Transient elastography: a new noninvasive method for assessment of hepatic fibrosis. Ultrasound Med Biol 29:1705–1713
21. Portney L, Watkins M (1999) Foundations of clinical research: application to practice. Prentice Hall, Upper Saddle River
22. Juluru K, Talal AH, Yantiss RK et al (2017) Diagnostic accuracy of intracellular uptake rates calculated using dynamic Gd-EOB-DTPA-enhanced MRI for hepatic fibrosis stage. J Magn Reson Imaging 45:1177–1185
23. Ning J, Yang Z, Xie S, Sun Y, Yuan C, Chen H (2017) Hepatic function imaging using dynamic Gd-EOB-DTPA enhanced MRI and pharmacokinetic modeling. Magn Reson Med 78:1488–1495
24. Bollow M, Taupitz M, Hamm B, Staks T, Wolf KJ, Weinmann HJ (1997) Gadolinium-ethoxybenzyl-DTPA as a hepatobiliary contrast agent for use in MR cholangiography: results of an in vivo phase-I clinical evaluation. Eur Radiol 7:126–132
25. Tschirch FT, Struwe A, Petrowsky H, Kakales I, Marincek B, Weishaupt D (2008) Contrast-enhanced MR cholangiography with Gd-EOB-DTPA in patients with liver cirrhosis: visualization of the biliary ducts in comparison with patients with normal liver parenchyma. Eur Radiol 18:1577–1586
26. Rohrer M, Bauer H, Mintorovitch J, Requardt M, Weinmann HJ (2005) Comparison of magnetic properties of MRI contrast media solutions at different magnetic field strengths. Invest Radiol 40:715–724
27. Hennedige TP, Wang G, Leung FP et al (2017) Magnetic Resonance Elastography and Diffusion Weighted Imaging in the Evaluation of Hepatic Fibrosis in Chronic Hepatitis B. Gut Liver 11:401–408
28. Feier D, Balassy C, Bastati N, Fragner R, Wrba F, Ba-Ssalamah A (2015) The diagnostic efficacy of quantitative liver MR imaging with diffusion-weighted, SWI, and hepato-specific contrast-enhanced sequences in staging liver fibrosis-a multiparametric approach. Eur Radiol. https://doi.org/10.1007/s00330-015-3830-0
29. Kovac JD, Dakovic M, Stanisavljevic D et al (2012) Diffusion-weighted MRI versus transient elastography in quantification of liver fibrosis in patients with chronic cholestatic liver diseases. Eur J Radiol 81:2500–2506

30. Wang QB, Zhu H, Liu HL, Zhang B (2012) Performance of magnetic resonance elastography and diffusion-weighted imaging for the staging of hepatic fibrosis: A meta-analysis. Hepatology 56: 239–247
31. Wang Y, Ganger DR, Levitsky J et al (2011) Assessment of chronic hepatitis and fibrosis: comparison of MR elastography and diffusion-weighted imaging. AJR Am J Roentgenol 196:553–561
32. Taouli B, Koh DM (2010) Diffusion-weighted MR imaging of the liver. Radiology 254:47–66
33. Luciani A, Vignaud A, Cavet M et al (2008) Liver cirrhosis: intravoxel incoherent motion MR imaging–pilot study. Radiology 249:891–899
34. Williamson KD, Chapman RW (2015) Editorial: further evidence for the role of serum alkaline phosphatase as a useful surrogate marker of prognosis in PSC. Aliment Pharmacol Ther 41:149–151
35. Al Mamari S, Djordjevic J, Halliday JS, Chapman RW (2013) Improvement of serum alkaline phosphatase to <1.5 upper limit of normal predicts better outcome and reduced risk of cholangiocarcinoma in primary sclerosing cholangitis. J Hepatol 58:329–334
36. Ponsioen CY, Chapman RW, Chazouilleres O et al (2016) Surrogate endpoints for clinical trials in primary sclerosing cholangitis: Review and results from an International PSC Study Group consensus process. Hepatology 63:1357–1367
37. Ehlken H, Wroblewski R, Corpechot C et al (2016) Spleen size for the prediction of clinical outcome in patients with primary sclerosing cholangitis. Gut 65:1230–1232
38. European Association for the Study of the L (2009) EASL Clinical Practice Guidelines: management of cholestatic liver diseases. J Hepatol 51:237–267
39. Huwart L, Sempoux C, Vicaut E et al (2008) Magnetic resonance elastography for the noninvasive staging of liver fibrosis. Gastroenterology 135:32–40
40. Lu PX, Huang H, Yuan J et al (2014) Decreases in molecular diffusion, perfusion fraction and perfusion-related diffusion in fibrotic livers: a prospective clinical intravoxel incoherent motion MR imaging study. PLoS One 9:e113846
41. Yoon JH, Lee JM, Baek JH et al (2014) Evaluation of hepatic fibrosis using intravoxel incoherent motion in diffusion-weighted liver MRI. J Comput Assist Tomogr 38:110–116
42. Haimerl M, Verloh N, Zeman F et al (2013) Assessment of clinical signs of liver cirrhosis using T1 mapping on Gd-EOB-DTPA-enhanced 3T MRI. PLoS One 8:e85658
43. Heye T, Yang SR, Bock M et al (2012) MR relaxometry of the liver: significant elevation of T1 relaxation time in patients with liver cirrhosis. Eur Radiol 22:1224–1232
44. Cassinotto C, Feldis M, Vergniol J et al (2015) MR relaxometry in chronic liver diseases: Comparison of T1 mapping, T2 mapping, and diffusion-weighted imaging for assessing cirrhosis diagnosis and severity. Eur J Radiol 84:1459–1465
45. Li Z, Sun J, Hu X et al (2016) Assessment of liver fibrosis by variable flip angle T1 mapping at 3.0T. J Magn Reson Imaging 43:698–703
46. Hinrichs H, Hinrichs JB, Gutberlet M et al (2016) Functional gadoxetate disodium-enhanced MRI in patients with primary sclerosing cholangitis (PSC). Eur Radiol 26:1116–1124
47. Keller S, Aigner A, Zenouzi R et al (2018) Association of gadolinium-enhanced magnetic resonance imaging with hepatic fibrosis and inflammation in primary sclerosing cholangitis. PLoS One 13:e0193929
48. Martin DR, Lauenstein T, Kalb B et al (2012) Liver MRI and histological correlates in chronic liver disease on multiphase gadolinium-enhanced 3D gradient echo imaging. J Magn Reson Imaging 36:422–429
49. Saito H, Tada S, Nakamoto N et al (2004) Efficacy of non-invasive elastometry on staging of hepatic fibrosis. Hepatol Res 29:97–103